Dielectric and optical properties of chitosan-Pb and chitosan-Bi nanocomposites

Ayman A. Zaki[1,2,*] [iD], T. A. Abdel-Basset[2,3,*], Mohammed Haggar[4,5], and Ali H. Bashal[5]

[1] *Department of Physics, Faculty of Science, Benha University, Benha, Egypt*
[2] *Department of Physics, Faculty of Science, Taibah University, Yanbu 46423, Saudi Arabia*
[3] *Department of Physics, Faculty of Science, Fayoum University, Fayoum 63514, Egypt*
[4] *Department of Chemistry, Faculty of Science, Alexandria University, Alexandria, Egypt*
[5] *Department of Chemistry, Faculty of Science, Taibah University, Yanbu 46423, Saudi Arabia*

ABSTRACT

In this work, chitosan was used as powerful chelating agent and an excellent template for synthesis of metal oxide nanoparticles. Chitosan-Pb and Chitosan-Bi nanoparticles have been synthesized by incorporating PbO/BiO nanoparticles within the chitosan matrix using a simple solution cast method. Dielectric and optical properties of the nanocomposite film were studied. Moreover, the effect of temperature on the dielectric properties of the hybrid film was determined. The absorption and transmittance were measured for the prepared samples by using UV–Vis spectrophotometer. The optical parameters such as refractive index, absorption coefficient, energy band gap, dispersion energy, oscillation energy, and the skin or penetration depth for the chitosan-PbO/-BiO nanocomposite were obtained.

1 Introduction

Natural polysaccharides often used as an ideal stabilizing agent have the requirements for low cost and renewable raw materials [1]. Nowadays, most of researchers have invented a lot of hybrid composite materials to gain new properties that fit many industrial applications [2]. In the last few decades, there is a growing interest to invent and design metal ion polysaccharide complexes that have been utilized for many useful applications like metal uptake, water treatment, forming novel catalysts, dyeing processes, and many other industrial applications [3].

Chitosan (CHIT) (Fig. 1) is a biopolymer (a biodegradable polysaccharide) derived from chitin by alkali deacetylation and is commonly found in nature, e.g., crustacean shells [4]. Due to its attractive properties, chitosan has attracted considerable attention in recent years as a promising material for applications such as modifier for the electrodes surfaces, excellent film forming capability, good stability, high water permeability, strong electrode surface adherence, biocompatibility, no toxicity, high

Address correspondence to E-mail: ayman_a73@hotmail.com; taa03@fayoum.edu.eg

Fig. 1 Structures of chitosan and chitin
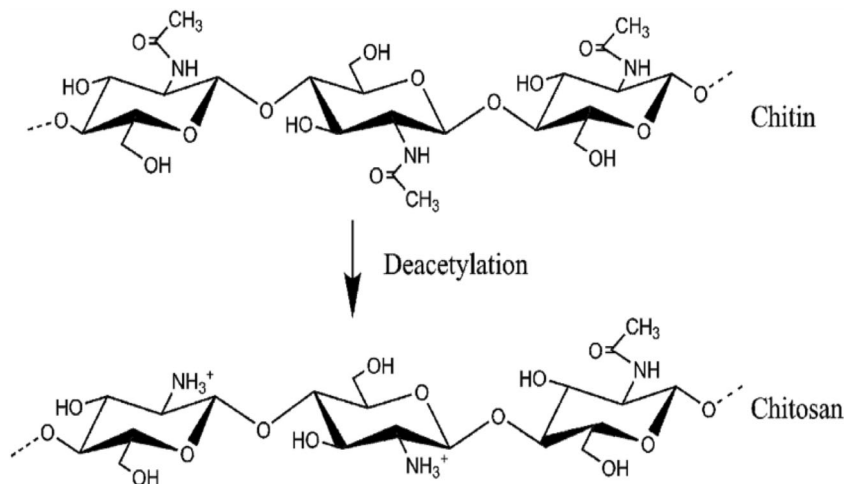
mechanical resistance, low cost, and susceptibility to chemical modifications due to the presence of reactive amino and hydroxyl functional groups from its structure [5, 6]. Chitosan and its derivatives, rather than any other polysaccharides, are considered as powerful template for the preparation of metal oxide nanoparticles owing to their unique ability to combine with metal ions via the hydroxyl and amino groups [7]. Nevertheless, many materials such as metal nanoparticles and carbon nanotube have been used with CHIT films to improve electric conductivity [8, 9].

Dielectric materials that possess high dielectric permittivity (ε) and dielectric field strength without excessive dielectric loss are necessary to meet the miniaturization requirements of microelectronic device structures, including gate dielectrics, high charge-storage capacitors and electro-active material [10]. The dielectric properties dependent effectively on the temperature and frequency applicable on the sample. At low temperatures, the dielectric materials aren't enough free charges, but when the temperature increases, more and more carriers can be passed on the top of barrier height and so yield an excess capacitance and conductance to measure of them under the external electric field [11, 12]. UV–vis absorbance characterization estimated the value of a direct energy band gap for BiFeO₃ and Chitosan-assisted BiFeO₃, respectively [13]. The optical, mechanical, and electrical properties of the chitosan/graphene nanoplatelets (CS/GNP) and chitosan/multi-walled carbon nanotube (CS/MWCNT) films were investigated [14]. Optical properties such as refractive indices spectra and band gap are studied

for the Cu nanoparticles with Chitosan host polymer [15]. Pb and Bi nanoparticles have promising electrical, chemical, thermal, and optical properties that attracted many scientists to study their utility in many applications [16, 17]. For the above reasons, in this study, we have synthesized chitosan-Pb and chitosan-Bi nanocomposite film and investigated the effect of bismuth and lead oxides nanoparticle on chitosan's conductivity, dialectical, and optical properties.

2 Experimental results and discussion

2.1 Materials and methods

Chitosan (powder, shrimp shells, product no. C3646, density = 0.15 – 0.3 g/cm³) and Bi₂O₃ (nanopowder, 90–201 nm particle size, 99.8% trace metals basis) were purchased from Sigma-Aldrich company. Pb₂O₃ (APS: 20–30 nm, purity 99.9%) was purchased from NANOSHEL.

2.2 Preparation of chitosan-metal oxide hybrid nanocomposites film

The hybrid Metal oxide chitosan nanocomposites were prepared using method of a one-pot solution casting. A 250 mg of chitosan powder (medium molecular weight) was dissolved in 20 mL of 2% (v/v) aqueous acetic acid solution under stirring for 6 h at room temperature. To this solution, 50 mg of metal oxides were added, and the mixture was sonicated for 6 h till a clear solution was achieved. The obtained viscous solution was casted in a Teflon Petri

dish and dried overnight at 60 °C for 2 h. The Petri dishes were then immersed into a 0.2 M sodium hydroxide solution for neutralization and phase separation. The solid films were dried in an oven adjusted at 80 °C for 6 h. Finally, the obtained films were then cleaned by several times washing with methanol and again were dried in an oven at 60 °C for 2 h. Furthermore, a pure chitosan film, without metal oxides, was prepared in a similar way for comparative study.

2.3 Measuring dielectric properties

We used "Solartron Frequency and Analytical Response analyzer" instrument for measuring the impedance spectra associated with our samples that were in the form of circular pellets and were ~ 1 mm thick and $\sim$ had 0.5 cm radius. The pellets were connected in series with small 47Ω resistor to stabilize the signal. The measurement frequency range was $f = 0.1$ kHz – 300 kHz at an AC amplitude of 0.3 V and zero DC voltage. The temperature was measured with a T-type thermocouple with its junction just in contact with the sample with accuracy better than $\pm$ 1 K. The dielectric permittivity (ε') was calculated as follows:

$$\varepsilon' = Cd/\varepsilon_o A \tag{1}$$

where C is the capacitance of the sample filled capacitor, d is the sample thickness, and ε_o is the vacuum permittivity, A is the electrode area. The electric modulus was given as follows [17]:

$$M^* = M' + iM'' \tag{2}$$

where the real and the imaginary components M' and M'', respectively, are $M' = \frac{\varepsilon'}{\varepsilon'^2 + \varepsilon''^2}$, $M'' = \frac{\varepsilon''}{\varepsilon'^2 + \varepsilon''^2}$ as a function of the dielectric permittivity and dielectric loss ($\varepsilon'' = \varepsilon' \tan \delta$). The ac conductivity ($\sigma_{ac}$) is calculated as a function of frequency as follows:

$$\sigma_{ac} = \omega \varepsilon_0 \varepsilon' \tan \delta \tag{3}$$

We used copper tapes as the electrodes that were fixed at the pellet with a thin layer of adhesive (with negligible contribution to the impedance) to avoid using a conducting paste (available to us was a silver paste) that would diffuse into the sample, resulting in unwanted signal in the impedance spectrum.

2.3.1 Dependent in frequency

The divergence of the dielectric permittivity ε' with frequency for CS-PbO and CS-BiO at various fixed temperatures is presented in Fig. 2.

It is shown that, the values of ε' decreases with increasing frequency for all samples, which might be associated with the decrease in the number of dipoles. Or the dipoles are no longer able to respond to the external electric field. The observed high dielectric permittivity in the low-frequency range is caused by the Maxwell–Wagner-type polarization. Also, the values of ε' or CS-PbO be exhibit relatively lower dielectric constant than CS-BiO [18]. The modulus formalism can be used to avert the contribution of the large value of the dielectric constant at low frequency to analyze the dielectric behavior of composites samples. The dielectric modulus M'' as a function of frequency for CS-PbO and CS-BiO at different temperatures is displayed in Fig. 3. It is shown that the values of low temperature tend to be zero referencing to the removal of the interfacial polarization. Also, one peak shows at high frequency for all sample which attributed to the conductivity current relaxation [19].

The peak of relaxation is observed and shifted to higher frequency with increasing temperature; these peaks may be attributed to the conductivity current relaxation. The relaxation time is calculated from the peak frequency via $\tau_{M\rho} = 1/2\pi f_{\rho m}$, to estimate its activation energy. Figure 4 displays the plot of log $\tau_{M\rho}$ with $1/T$. As shown, ρ relaxation shows an Arrhenius temperature dependence of its relaxation time. The solid line in Fig. 4 is the fitted result following Arrhenius law $\tau = \tau_o \exp(-E_a/kT)$, where τ_o, E_a, k, and T are high-temperature limit of relaxation, activation energy, Boltzmann's constant, and the absolute temperature, respectively. The calculated value of E_a is 0.377 eV and 0.652 eV for CS-PbO and CS-BiO, respectively; this value indicated to the ionic materials [20].

The ac conductivity dependence of frequency can be calculated by ($\sigma_{ac} = \omega \varepsilon_0 \varepsilon' \tan \delta$), where ω is the angular frequency, ε_0 is the permittivity of the free space, and $tan\delta$ is the loss tangent. Figure 5 shows the frequency dependence of σ_{ac} for CS-PbO and CS-BiO composites at versus temperatures.

For CS-PbO and CS-BiO composites, the ac conductivity increases linearly by increasing frequency, this is due to increases of the absorbed energy which
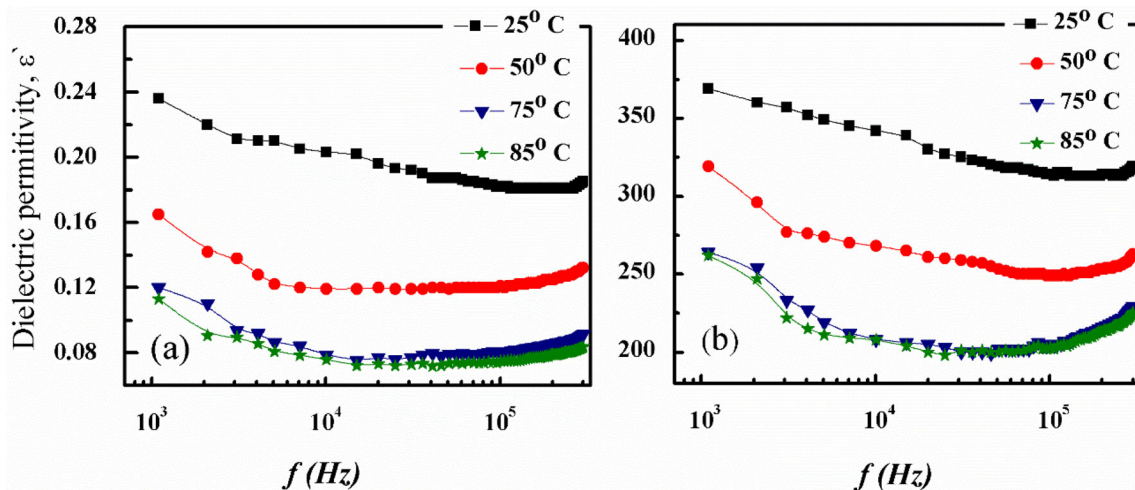
Fig. 2 Frequency dependence of dielectric permittivity ε' for (**a**) CS-PbO and (**b**) CS-BiO at different temperatures
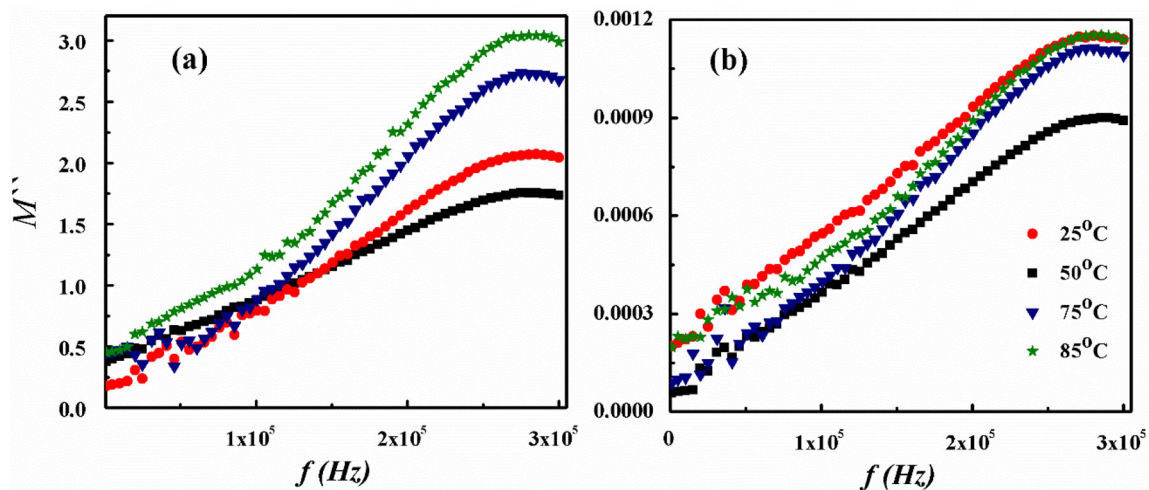

Fig. 3 Frequency dependence of M'' for (**a**) CS-PbO and (**b**) CS-BiO at different frequencies
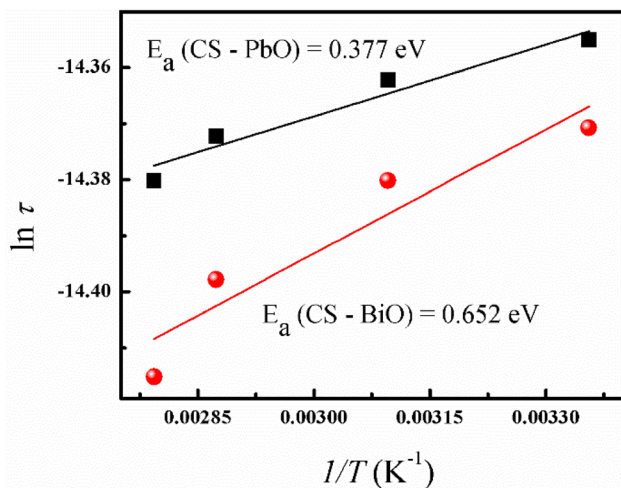

Fig. 4 The variation of $\ln(\tau)$ versus 1000/T for CS-PbO and CS-BiO

leads to increase the charge carriers that contributed to the conduction process. The ac conductivity dependence of frequency is given by ($\sigma_{ac} = B\omega^s$), where s is the universal exponent, which explains to understand the conduction mechanism for CS-PbO and CS-BiO composites. The variation of $\ln(\sigma_{ac})$ versus ln (f) at different temperatures are shown in Fig. 6. The values of s were obtained from the slopes of the red lines as shown in Fig. 6a and b and listed in Table 1.

We show that the values of s were larger than unity and increase with increasing temperatures. This means that small polaron tunneling (SPT) is the suitable conduction mechanism for CS-PbO and CS-BiO composites [21].

Fig. 5 Frequency dependence of σ_{ac} for (**a**) CS-PbO and (**b**) CS-BiO at different temperatures
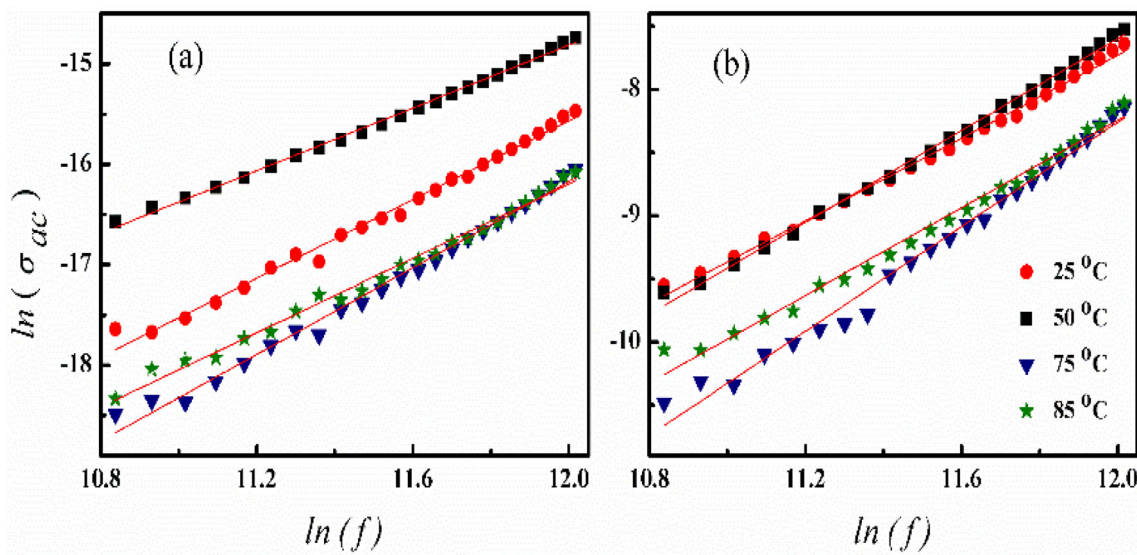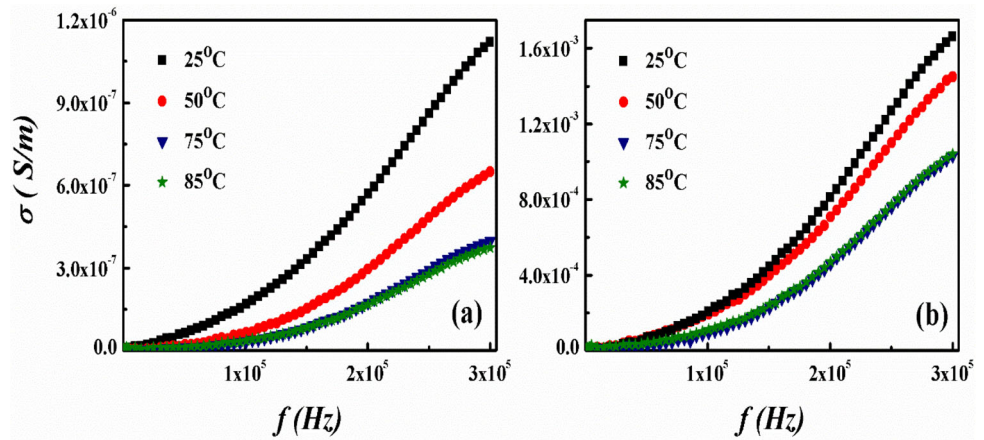

Fig. 6 The variation of $\ln(\sigma_{ac})$ dependence of frequency for (**a**) CS-PbO and (**b**) CS-BiO at different temperatures, and the solid line is the fitting according to ($\sigma_{ac} = B\omega^s$)

Table 1 The values of the exponent s for CS-PbO and CS-BiO at different temperatures

Temperature	CS-PbO	CS-BiO
25 °C	1.56067	1.63675
50 °C	1.6502	1.73403
75 °C	1.7523	1.8766
100 °C	1.8581	1.96963

2.4 Measuring optical properties

The optical spectroscopic analyses of the prepared samples have been carried out by using UV–visible–near IR spectroscopy (UV-1800 SHIMADZU, Japan) over the wavelength range of (190–1100 nm). Figure 7 shows the wavelength dependence of the absorption spectra for the CS, CS-BiO, and CS-PbO nanocomposites, where the absorption increases by mixing of PbO and BiO nanoparticles within the chitosan. Also, it shows the wavelength dependence of the transmission spectra for CS, CS-BiO, and CS-PbO nanocomposite samples. Unlike the pure CS, the samples CS-BiO and CS-PbO were slightly increasing their transmittance with wavelength due to increase in the sample crystallization. It was observed that no peaks were observed within the studied wavelength range (190–1100 nm) for CS-BiO and CS-PbO nanocomposite samples which confirm the increase in the sample crystallization also.
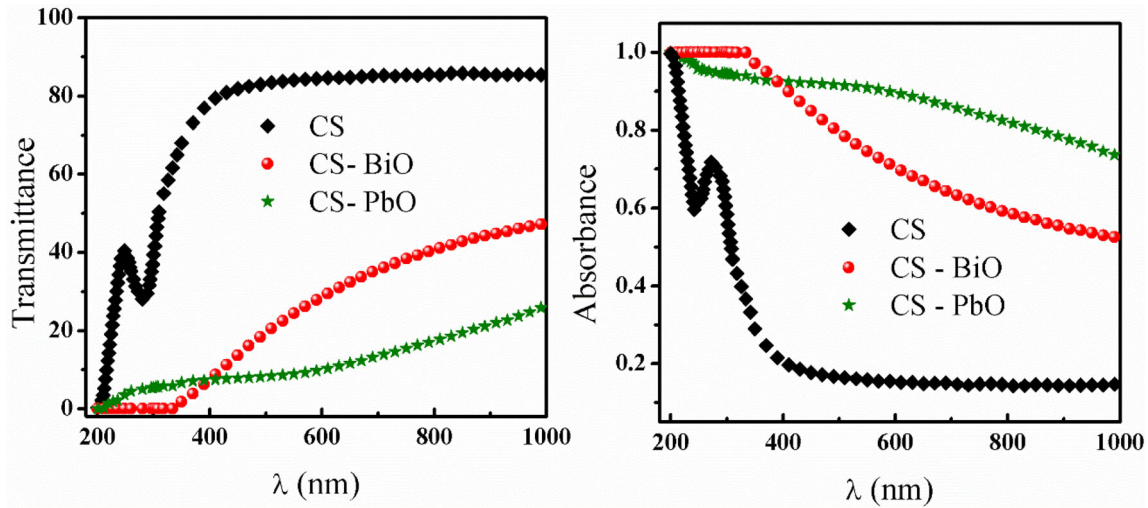
Fig. 7 Optical absorbance and transmittance spectra of CS, CS-BiO, and CS-PbO

2.4.1 Absorption coefficient and Energy band gap

The absorption coefficient (α) can be obtained by knowing the absorbance A and the sample thickness t as follows [22]:

$$\alpha = (2.303) \times \frac{A}{t} \tag{4}$$

The thickness of CS, CS-BiO, and CS-PbO films were measured by using the optical microscope. The energy band gap E_g was calculated from the absorption coefficient α as follows [23–25]:

$$\alpha h = B\left(h - E_g\right)^n \tag{5}$$

where h is the constant of Planck, v is the frequency of the incident light, B is a constant, and n is an index depending on the nature of the electronic transition. The best fit was found when n is equal to 2 for the allowed indirect transition process. From Eq. (5), E_g of CS, CS-BiO, and CS-PbO nanocomposites were obtained from the extrapolation of the straight-line portion of the photon energy (hv) as shown in Fig. 8 and listed in Table 2. It was observed that the values of E_g decrease by doping BiO and PbO within CS material which can be used in many applications such as solar energy and organic photovoltaics.

2.4.2 Urbach Energy and steepness parameter

The key attribute of the amorphous material absorption edge is an exponential increase in the absorption coefficient with photon energy where the edge of absorption is called the Urbach edge. Urbach
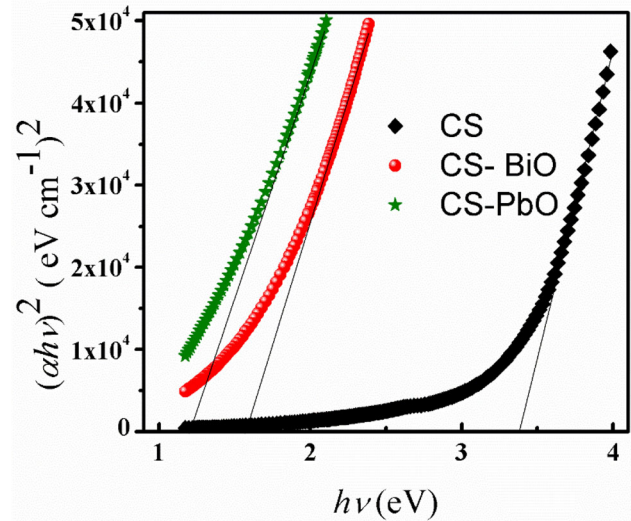

Fig. 8 The plot of $(\alpha hv)^2$ versus photon energy (hv) of all samples

Energy distinguishes the exponential tail size of absorbance edge. The Urbach energy (E_U) refers to the band tail width of the localized states, and the exponential absorption tails are given in the experimental relationship as follows [26, 27]:

$$\alpha = \alpha_o e^{(hv/E_U)} \tag{6}$$

$$\ln \alpha = \ln \alpha_o + \frac{hv}{E_U} \tag{7}$$

where α_o is a constant. From Eq. 4, the Urbach energy (E_U) can be obtained for the samples used by plotting the relation between ($Ln\alpha$) and the photon energy (hv) as shown in Fig. 9 and listed in Table 2. It was observed that E_U increases with doping BiO and PbO

Table 2 The energy band gap E_g, the Urbach energy E_U, steepness parameters S, the dispersion energy E_d, the oscillator energy E_o, and the refractive index at infinite wavelength n_∞ for all samples used

Sample	E_g (eV)	E_U (eV)	S ($\times 10^{-2}$)	E_d (eV)	E_o (eV)	n_∞
CS	3.40	2.45	0.16	9.82	8.15	1.48
CS-BiO	1.60	5.98	0.43	14.89	6.58	1.81
CS-PbO	1.12	16.10	1.05	6.74	4.58	1.57

which may be due to increase in the defect states density of CS-BiO and CS-PbO nanocomposite films [28, 29].

The steepness parameter S can be determined at room temperature ($T = 300$ K) as follows [30]:

$$S = \frac{K_B T}{E_U} \qquad (8)$$

where K_B is Boltzmann constant and the values of S for CS, CS-BiO, and CS-PbO films are given in Table 2.

The thickness of the skin or depth of penetration influences the essence of the interaction between an incident light wave and the electrons in the materials. The skin or depth of the penetration γ is obtained by the relationship [31, 32]:

$$\gamma = \frac{1}{\alpha} = \frac{\lambda}{4\pi k} \qquad (9)$$

The variation of γ of CS, CS-PbO, and CS-BiO thin films with $h\nu$ is shown in Fig. 10. It was observed that the γ is large at lower energy range and varies with the thickness of the film. At higher energy range, the γ is lower due to the energy loss by increasing the electron collisions [33].
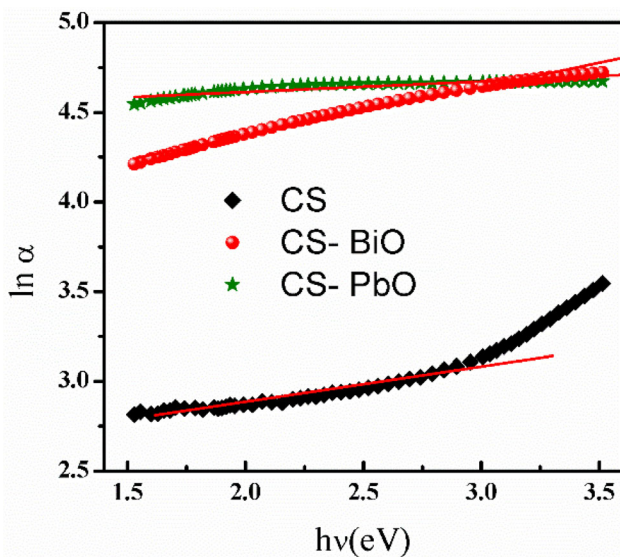
2.4.3 Refractive index and optical dispersion parameters

Refractive index plays a major role in the science of materials and several optical technologies. Refractive index can be measured using UV–Vis spectrophotometer to know the absorption, transmission, and reflection of the materials. Figure 11 shows the refractive index and wavelength dispersion relation for pure CS, CS-PbO, and CS-BiO nanocomposites. The values of refractive index were increased noticeably by doping PbO and BiO nanocomposites in the CS film as shown in Fig. 11. The doping of PbO and BiO nanoparticles through the CS host makes the nature of new material denser and changes the internal microstructure of the film which leads to high refractive index [33–35]. High values of the refractive index for new films will allow it to use in many optical applications including wave guides and light emitting diodes [36].

The real values of refractive index as a function of photon energy through the transparent region of spectrum can be used for determining many optical dispersion parameters such as the dispersion energy
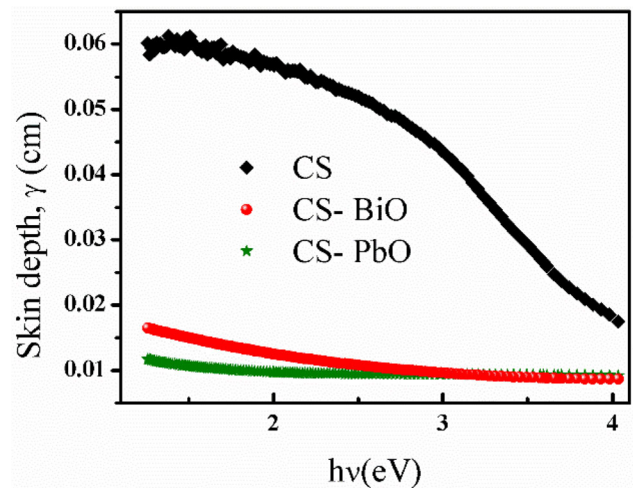

Fig. 9 The relation between ($Ln\alpha$) and the photon energy ($h\nu$) for all samples

Fig. 10 Depth of the skin, γ against the energy photon, and $h\nu$ for all films used
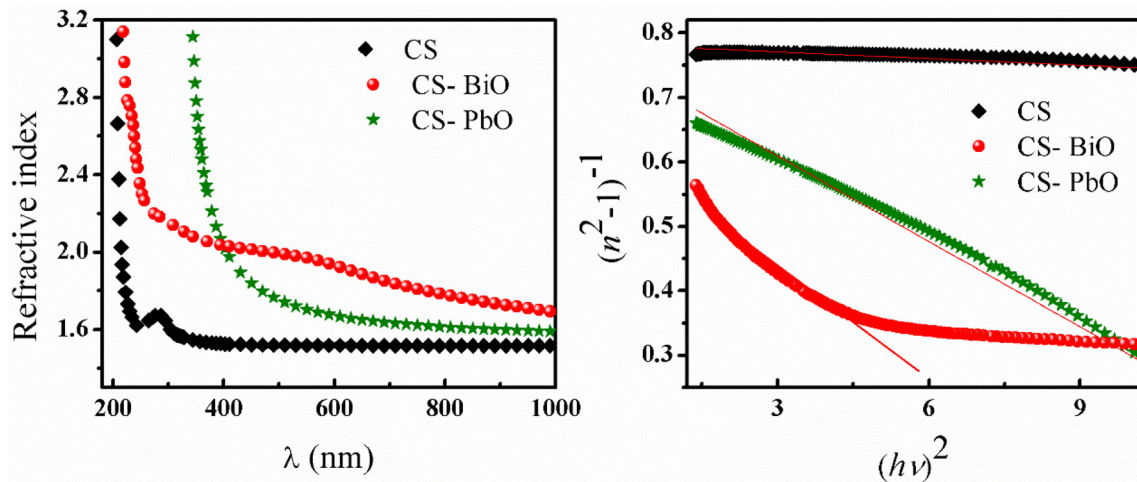
Fig. 11 The refractive index dispersion with wavelengths and the relation of $(n^2-1)^{-1}$ versus $(hv)^2$ for all samples

E_d, the single oscillator energy E_o, and the long wavelength refractive index n_∞.

Wemple-DiDomenico describes the single oscillator model to define the energy dispersion parameters E_d and E_o which calculate the average strength of the optical interband transitions and the energy separation between the valence and conduction bands, respectively, by the following relation [23, 37–40]:

$$n^2 = 1 + \frac{E_d E_o}{E_o^2 - (h)^2} \tag{10}$$

$$(n^2 - 1)^{-1} = \frac{E_o}{E_d} - \frac{(h)^2}{E_d E_o} \tag{11}$$

By plotting $(n^2-1)^{-1}$ versus $(hv)^2$ from Eq. (11), E_o and E_d values were determined from the slope and the intercept of the linear fitting for CS, CS-PbO, and CS-BiO nanocomposite as in Fig. 11 and listed in Table 2.

The index of refraction at infinite wavelength (n_∞) due to the electronic transition can be obtained by substituting λ equal to infinite in Eq. 10 as follows [41, 42]:

$$n_\infty^2 = 1 + \frac{E_d E_o}{E_o^2} \tag{12}$$

And then:

$$n_\infty = \sqrt{1 + \frac{E_d}{E_o}} \tag{13}$$

The values of n_∞ were calculated by knowing the values of E_0 and E_d for the CS, CS-PbO, and CS-BiO samples as in Table 2.

3 Conclusion

Chitosan-Pb and chitosan-Bi nanocomposite film have been synthesized by incorporating metal oxide molecules within the chitosan matrix using a simple solution cast method. The dielectric properties for CS-PbO and CS-BiO composite as a function of temperature and frequency were studied. The values of dielectric permittivity for CS-BiO exhibit relatively lower dielectric constant than CS-PbO. Relaxation peaks have been recognized and shifted to higher frequency with increasing temperature corresponding to ρ relaxation process. The activation energy E_a is 0.377 eV and 0.652 eV for CS-PbO and CS-BiO, respectively, calculated by Arrhenius relation, which indicated to the ionic materials. The ac conductivity of for CS-PbO and CS-BiO increases with increasing frequency. The conduction mechanism could be small polaron tunneling. The optical properties of the CS, CS-PbO, and CS-BiO nanocomposites were investigated. The addition of PbO and BiO nanoparticles within the CS material are affected by the optical absorbance and transmittance. The values of energy band gap were decreased by blending PbO and BiO nanoparticles within CS material which can be used in some optical applications such as optoelectronic devices. The optical dispersion parameters such as dispersion energy, oscillation energy, the skin or penetration depth, and refractive index in visible region and at high wavelength were calculated.

Compliance with ethical standards

Conflicts of interest The authors declare no conflict of interest.

References

1. C. Vilela, R. J. B. Pinto, S. Pinto, P. Marques, A. Silvestr, Polysaccharides-Based Hybrids with Metal Nanoparticles, Polysaccharide Based Hybrid Materials, ch2 9–30 (2018).
2. G. Kickelbick, Prog. Polym. Sci. **28**, 83–114 (2003)
3. T. Xu, J. Membr. Sci. **263**, 1–29 (2005)
4. M. Dash, F. Chiellini, R.M. Ottenbrite, E. Chiellini, Prog. Polym. Sci. **36**, 981–1014 (2011)
5. Wu, Li-Qun, P. Anand Gadre, Yi Hyunmin, J. Mark Kastantin, W. Gary Rubloff, E. William Bentley, F. Gregory Payne, and Reza Ghodssi, Langmuir 18, 8620–8625 (2002).
6. A.J. Varma, S.V. Deshpande, J.F. Kennedy, Carbohyd. Polym. **55**, 77–93 (2004)
7. S.M. Riyadh, K.D. Khalil, A.H. Bashal, Catalysts **10**, 100 (2020)
8. K. Asadpour-Zeynali, F. Mollarasouli, Cent. Eur. J. Chem. **12**, 711–718 (2014)
9. Y.L. Liu, W.H. Chen, Y.H. Chang, Carbohyd. Polym. **76**, 232–238 (2009)
10. C. Zhang, Q. Chi, J. Dong, Y. Cui, X. Wang, L. Liu, Q. Lei, Scientific reports **6**, 33508 (2016)
11. C. Bilkan, S. Altındal, Y. Azizian-Kalandaragh, Phys. B **515**, 28 (2017)
12. A. Nikravan, Y. Badali, Ş Altındal, I. Uslu, I. Orak, J. Electron. Mater **46**, 5728 (2017)
13. M. Safwan Sazali, et al, Results in Physics 15, 102740 (2019).
14. O.B. Mergen, E. Arda, G.A. Evingur, J. Compos. Mater. **54**, 1497–1510 (2019)
15. B. Aziz Shujahadeen, Nanomaterials, 7, 444 (2017).
16. Anu, K. Yadav, Materials Today: Proceedings, 15 February (2020). https://doi.org/10.1016/j.matpr.2020.01.467.
17. M. Abid, M. Et-tabirou, M. Taibi, Mater. Sci. Eng. B **97**, 20–24 (2003)
18. M. Hdidar, S. Chouikhi, A. Fattoum, M. Arous, A. Kallel, J. Alloy. Compd. **750**, 375–383 (2018)
19. T.A. Abdel-Baset, A. Hassen, Phys. B **499**, 24–28 (2016)
20. A. Abou Elfadl, A. M. Ismail & M. I. Mohammed, Journal of Materials Science: Materials in Electronics 3, 8297–8307 (2020).
21. R.B. Belgacem, M. Chaari, A. Matoussi, J. Alloy. Compd. **651**, 49–58 (2015)
22. S.A. Khan, J.K. Lal, A.A. Al-Ghamdi, Opt. Laser Technol. **42**, 839–844 (2010)
23. J. Tauc, R. Grigorovici, A. Vencu, Phys. Status. Solidi. B **15**, 627–637 (1996)
24. E.M. El-Menyawy, A.A.A. Darwish, I.T. Zedan, Opt. Laser Technol. **79**, 158–163 (2016)
25. D. Bhattacharyya, S. Chaudhuri, A.K. Pal, Vacuum **43**, 313–316 (1992)
26. F. Urach, Phys. Rev. **92**, 1324 (1953)
27. M. Abdel-Baki, F. El-Diasty, Curr. Opin. Solid State Mater. Sci. **10**, 21–29 (2006)
28. N. Banu, A.H. Bhuiyan, K.S. Hossain, Adv. Polym. Technol. **37**, 84–94 (2018)
29. S.A. Fayek, M.R. Balboul, K.H. Marzouk, Thin Solid Films **515**, 7281–7285 (2007)
30. H. Mahr, Cryst. Phys. Rev. **125**, 1510–1516 (1962)
31. H. Eugene, Optics, fourth edition, Adelphi University, San Francisco, Boston, New York, (2002), Ch 4. P. 139.
32. J.I. Pankove, *Optical Processes in Semiconductors* (Dover Publications Inc., New York, 1975).
33. P.W. Gilberd, J. Phys. F Met. Phys. **12**, 8 (1982)
34. H. Eugene, *Optics*, 4th edn. (Adelphi University, San Francisco, Boston, New York, 2002), p. 113
35. A.A. Zaki, M. Hagar, N.R.E. Radwan, Optik **139**, 95–103 (2017)
36. O.G. Abdullah, S.B. Aziz, K.M. Omer, Y.M. Salih, J. Mater. Sci. **26**, 3–9 (2015)
37. T.G. Urs, G.K. Gowtham, M.B. Nandaprakash, D. Mahadevaiah, Y. Sangappa, R. Somashekar, Indian J. Phys. **91**, 53–60 (2017)
38. R.T. Potzsch, B.C. Stahl, H. Komber, C.J.H.B.I. Voit, Polym. Chem. **5**, 11–21 (2014)
39. A.A. Zaki, A.A. El-Amin, Opt. Laser Technol. **97**, 71–76 (2017)
40. W. Sellmeier, Ann Phys Chem. **143**, 271 (1871)
41. S.H. Wemple, M. DiDomenico, Phys. Rev. B **3**, 38–51 (1971)
42. S.H. Wemple, M. DiDomenico, Phys. Rev. Lett. **23**, 1156 (1969)